Article citation info:
Chaourar H. H, Iratni A, Laroussi K. Nonlinear observer-based fault diagnosis in photovoltaic systems integrated with voltage source converters using an extended Kalman filter. Diagnostyka. 2026;27(2):2026208. https://doi.org/10.29354/diag/224223.

DIAGNOSTYKA, 2026, Vol. 27, No. 2

e-ISSN 2449-5220
DOI: 10.29354/diag/224223

NONLINEAR OBSERVER-BASED FAULT DIAGNOSIS IN PHOTOVOLTAIC SYSTEMS INTEGRATED WITH VOLTAGE SOURCE CONVERTERS USING AN EXTENDED KALMAN FILTER

Hanene Hanene CHAOURAR [1, *], Abdelhamid IRATNI [2], Kouider LAROUSSI [1]

[1] Applied Automation and Industrial Diagnostics Laboratory, Faculty of Science and Technology, University of Djelfa 17000 DZ, Algeria
[2] Department of Electrical Engineering, Faculty of Science and Technology, University Mohamed El Bachir El Ibrahimi of Bordj Bou Arreridj,34030 DZ, El Anasser, Bordj Bou Arreridj, Algeria
[*] Corresponding author, e-mail: chorarehanane@gmail.com

Abstract

With the rapid penetration of renewable generation, the stability and operability of photovoltaic (PV) systems increasingly depend on reliable fault diagnosis mechanisms. This work develops a nonlinear observer-based diagnostic framework for PV systems interfaced through a voltage source converter (VSC). The approach formulates a nonlinear state-space model of the PV converter system and deploys an Extended Kalman Filter (EKF) for real-time state estimation and sensor fault detection, targeting voltage and current measurements under varying operating conditions. The contribution does not rest on the EKF formulation itself, but on its integration within a unified estimation diagnosis control structure. The estimator generates residuals that enable rapid fault detection while simultaneously supporting measurement correction to maintain control performance. This coupling ensures continuity of maximum power point tracking (MPPT) even in the presence of sensor degradation. Simulation results demonstrate a reduction of estimation error by up to 99.9% for both voltage and current states, with fault detection occurring within milliseconds. The MPPT efficiency remains above 95% under faulty conditions, while output power exhibits improved stability compared to non-diagnosed configurations. The inclusion of the VSC further enhances dynamic response and robustness to environmental variability. These results confirm that the proposed observer-based architecture strengthens diagnostic reliability while preserving system performance in real time.

Keywords: nonlinear observer, fault diagnosis, extended Kalman filter, sate estimation, photovoltaic systems.

List of Symbols/Acronyms

EKF – Extended Kalman Filter;
MPPT – Maximum Power Point Tracking;
VSC – Voltage Source Converters;
iRES – individual renewable energy;
SPV – Solar Photovoltaic;
CSP – Solar thermal power;
PV – Photovoltaic;
SMO – Sliding Mode Observer;
SMC – Sliding Mode Control;
RMS – Root Mean Square;
ANN – Artificial Neural Network;
MPP – Maximum Power Point;
FDD – Fault Detection and Diagnosis;
FTC – Fault Tolerant Control;
P&O – Perturb and Observe;
INC – Incremental Conductance;
I_{pv} – The photovoltaic Current;
I_{ph} – The light emilting Current;
I_o – The saturation Current;
q – The electron charge;
V_{pv} – The PV source voltage;
R_s – Series resistance;
R_{sh} – Shunt resistances;
k– The Boltzmann constant;
n – The ideality factor;
T – The Temperature of the junction;
Z_k – The measurement vector;
A – Derivative of the model;
y_k – The measurement Residual;
H_k – The measurement Jacobian;
K_k – Kalman gain;
T_s – Sampling time;
u_k – input;
s – The Laplace variable;
$Th_{(i,v)}$ – Thresholds;
C – The observation matrix;
$\sigma_{(i,v)}$ – The standard deviations;
α – The tuning coefficient;
V_{out} – The converter output voltage;
I_c – The capacitor current;
f – The grid frequency.

Received 2025-12-07; Accepted 2026-06-05; Available online 2026-06-16

1. INTRODUCTION

The transition toward sustainable energy systems has intensified the deployment of renewable generation, particularly solar and wind, to meet escalating electricity demand [1]. Individual renewable energy sources (iRES) contribute not only to generation capacity but also to system reliability and stability. Energy, beyond its technical dimension, underpins socioeconomic development and quality of life; yet, the rapid expansion of energy-intensive activities continues to strain finite resources. In this context, the International Renewable Energy Agency (IRENA) identifies clean energy technologies as essential instruments for mitigating climate change. Under fluctuating weather conditions, hybridization of renewable sources smooths power variability, while energy storage systems complement generation units to improve efficiency and limit waste [2].

Most renewable technologies ultimately derive from solar radiation. Among them, solar energy stands out for its global availability, low environmental impact, and technological maturity. Electricity generation from solar resources is achieved through solar photovoltaic (SPV) systems or concentrated solar thermal power (CSP) plants, the latter converting thermal energy into mechanical work. SPV systems, by contrast, directly convert irradiance into electricity via photovoltaic (PV) cells, forming the core of modern solar installations [3]. The sector continues its rapid expansion; projections indicate that PV could supply a substantial share of global electricity by 2030, driven by low operational costs and minimal maintenance requirements.

Despite this growth, PV system performance remains tightly coupled to measurement accuracy. Sensor malfunctions particularly in voltage and current channels introduce erroneous inputs that propagate through control loops, degrade maximum power point tracking (MPPT), and, in severe cases, compromise system integrity [4]. The diagnostic challenge is compounded by environmental variability: fluctuations in irradiance and temperature produce transient responses that may resemble fault signatures, obscuring clear discrimination [5, 6]. Increasing system scale and interconnection density further amplify this complexity, while hardware constraints limit the deployment of high-resolution diagnostic schemes [7].

Economic considerations impose an additional constraint. Advanced diagnostic frameworks often entail non-negligible implementation costs, which can restrict their adoption in cost-sensitive installations. As noted in recent studies, the trade-off between diagnostic precision and economic feasibility remains a decisive factor in practical deployments.

Sensors form the backbone of PV monitoring and control, encompassing irradiance sensors, temperature probes, and voltage and current transducers [8]. Their failure directly affects critical functions. MPPT algorithms, for instance, rely on accurate electrical measurements to identify optimal operating points; deviations in sensor readings lead to suboptimal tracking and reduced energy yield. Monitoring systems, similarly, depend on reliable data to detect shading effects, degradation, or electrical anomalies. Faulty measurements may therefore result in false alarms or undetected failures [9]. Predictive maintenance strategies, which rely on continuous data streams, are particularly sensitive to such inaccuracies, potentially triggering unnecessary interventions or masking genuine degradation [10, 11].

Conventional fault diagnosis techniques threshold-based methods, physical model-based approaches, statistical analysis, and signal comparison each exhibit inherent limitations. Threshold-based schemes offer simplicity but lack robustness in noisy environments and often fail to detect incipient faults [12, 13]. Model-based methods achieve high accuracy when system parameters are well known; however, their applicability diminishes in large-scale or dynamically varying systems. Statistical approaches depend heavily on historical data, which may be unavailable or non-stationary [8, 14]. Signal comparison techniques, while effective in principle, increase system complexity and cost.

More advanced frameworks have therefore been proposed, including Extended Kalman Filters (EKF) [15], artificial neural networks [16, 17], and machine learning techniques [18]. Sliding Mode Observers (SMOs) have also been investigated, offering robustness at the expense of sensitivity to parameter variations, susceptibility to chattering, and limited effectiveness for progressive faults [19, 20]. Recent work emphasizes the need for early, noise-resilient detection mechanisms capable of operating under rapidly changing conditions [21, 22].

Against this backdrop, the present study develops a nonlinear observer-based diagnostic framework built upon the Extended Kalman Filter. The choice of EKF is not incidental. Photovoltaic systems exhibit pronounced nonlinearities arising from the exponential current voltage characteristic, environmental dependencies, and converter dynamics; linear Kalman filtering is therefore inadequate. The EKF, through local linearization via the Jacobian, provides consistent state estimates under such conditions. These estimates, in turn, enable the generation of reliable residuals, forming the basis for fault detection [16].

The proposed framework integrates three tightly coupled functions within a single structure: nonlinear state estimation, residual-based fault detection with adaptive thresholding, and real-time measurement correction. An intelligent switching mechanism replaces faulty sensor readings with EKF estimates as soon as a fault is confirmed, thereby preserving MPPT performance and ensuring

operational continuity [23, 24]. This integration distinguishes the approach from existing methods, which typically address estimation, detection, and correction in isolation.

A comparative analysis, summarized in Table I, positions the EKF-based observer against alternative techniques. Data-driven methods such as ANN achieve high classification accuracy but require extensive training datasets and lack interpretability. Threshold-based approaches remain computationally efficient yet suffer from poor robustness. SMO-based methods provide fast response but are affected by chattering and noise sensitivity. In contrast, the EKF observer achieves low RMS estimation error, rapid fault detection, and adaptability to environmental variations, making it well suited for real-time PV monitoring.

The effectiveness of the proposed approach is validated through simulation under diverse fault scenarios. Results indicate a reduction of estimation error by up to 99.9% for voltage and current, fault detection within milliseconds, and sustained MPPT efficiency exceeding 95%. Power output stability is likewise improved relative to non-diagnosed configurations. These results confirm that integrating estimation, diagnosis, and correction within a unified EKF-based framework enhances both reliability and operational resilience.

While prior studies have largely focused on mechanical faults, shading effects, and module degradation, comparatively limited attention has been given to voltage and current sensor faults and their direct impact on MPPT and control performance [25]. Existing approaches often rely either on filtering techniques without explicit fault isolation or on data-driven models that lack real-time corrective capability.

The remainder of the paper is organized as follows. Section 2 presents the system modelling and EKF formulation. Section 3 examines the impact of sensor faults and details the detection strategy. Section 4 describes the proposed diagnostic architecture and control integration. Section 5 discusses the simulation results. Section 6 concludes the study.

1.1. Research contribution

This work advances the state of PV fault diagnosis through a unified, observer-based framework with the following contributions:

- A comprehensive EKF-based diagnostic architecture is developed, integrating real-time state estimation, residual generation, adaptive thresholding, and automated fault detection within a single structure.
- A nonlinear PV model with a corrected analytical Jacobian is derived and embedded within the EKF, improving estimation accuracy relative to conventional formulations.
- An adaptive residual-based threshold is introduced, enabling reliable fault detection under varying irradiance and temperature conditions while mitigating false alarms.
- A rule-based signal-switching mechanism is implemented, ensuring seamless replacement of faulty measurements with EKF estimates and preserving MPPT performance.
- A quantitative comparison with ANN- and SMO-based methods demonstrates that the proposed approach achieves comparable or superior performance without reliance on training data or high-gain tuning, supporting its suitability for real-time deployment.

2. METHODOLOGY: MODELLING, ESTIMATION

2.1. Photovoltaic (PV) system modelling

A typical photovoltaic (PV) system comprises several components, including solar panels, inverters, and sensors. In this study, we employ a nonlinear model that captures the dynamics of currents and voltages within the system. The model incorporates critical factors such as solar irradiance, ambient temperature, and load resistance, all of which significantly influence sensor performance. A robust modelling framework is essential to ensure accurate and reliable estimations when applying diagnostic techniques [21]. Our approach to modelling PV generation is based on the diode solar cell model, which is widely used for representing various PV module technologies due to its high predictive accuracy. The system behaviour is described by the following equation:

$$I_{pv} = I_{ph} - I_o\left[e\left(\frac{q(V_{pv}+R_sI_{pv})}{nkT}\right)-1\right] - \frac{V_{pv}+R_sI_{pv}}{R_{sh}} \quad (1)$$

Where I_{ph} is the light emitting current, $I_o$represents the saturation current and n is the ideality factor of the diode. Constant q is the absolute value of electron's charge (-1.602117646×10^ (-19) C), k is the Boltzmann's constant (-1.380653×10^ (-23) J/K), while T is the temperature of the junction (K). Also, R_s and R_{sh}series and shunt resistances.

For system modelling, simulation, and implementation of the (MPPT) algorithm, we utilize the YGE 60 Cell Series module (YL245P-29b) from Suntech. This module was characterized under standard test conditions (1000 W/m², 25°C). Table II summarizes its electrical specifications.

The PV module behaves as a current source dependent on irradiance and temperature. These variables induce nonlinear I–V characteristics that evolve with environmental conditions. As shown in Figure 1, the (MPP) is not fixed but varies with changes in irradiance and temperature. An effective MPPT controller must therefore dynamically track the MPP to maximize energy extraction from the array.

Table 1. Performance comparison of fault detection and diagnosis techniques in PV systems

Method	Approach	Algorithms Used	Key Advantages	Key Limitations	Performance Metrics	Reference
ANN-Based Fault Detection	Data-driven, pattern recognition	Artificial Neural Networks (ANN)	- Handles nonlinearities well - No need for precise models - Scalable for large systems Captures nonlinearities, high accuracy	- Requires extensive training data - Black-box nature - Requires large dataset, no interpretability, no real-time correction	-Detection Accuracy: 93.09%Classification - Accuracy: 95.44%. RMS 0.193–0.365%	Zamzeer et al., 2023[32]
Threshold-Based Methods	Rule-based, static thresholds	Statistical analysis	- Simple implementation - Low computational cost	- Poor performance in noisy environments - High false alarms - Fixed thresholds	- Accuracy: ~70-80% - False positives: High	El-Banby et al., 2023[8]
Sliding Mode Observers (SMO)	Robust control, fault isolation	Sliding Mode Control (SMC)	- Robust to disturbances - Fast response	- High chattering - Sensitive to parameter variat-ions - Poor for progressive faults	- Detection time: ~0.05 s - Noise sensitivity: High	Criollo et al., 2022[22]
Ensemble Machine Learning	Hybrid data-driven approach	PCA, Neural Networks	- Combines multiple models for better accuracy - Reduces overfitting	- Complex implementation - High computational load	- Average error: <2.0% - Scalability: Moderate	Raj, V et all [33]
Physical Model-Based Methods	Physics-based, analytical models	Mathematical modelling	- High accuracy if model is precise - Good for known fault types	- Not suitable for complex/dynamic systems - Requires exact parameters	- Accuracy: ~85-90% - Flexibility: Low	Spataru et al., 2015[15]
Standard Kalman Filter (KF)	Li near model-based	Linear system required	Optimal for linear systems, simple	Not suitable for nonlinear PV systems	Estimation only (limited fault detection)	Simon D [30]
EKF-Based Observer	Nonlinear observer, state estimation	Extended Kalman Filter (EKF)	- 99.9% reduction in RMS error - Real-time fault detection (milliseconds) - MPPT efficiency >95% - Adaptive thresholding	- Requires accurate system modeling - Computational complexity	- Voltage RMS: ~0.11 V - Current RMS: ~0.002 A - Detection time: ~0.015 s	Proposed Study

Table 2 Characteristics of the PV module YGE 60 Cell Series (YL245P-29b).

Parameters	Value
Maximum Power	245 W
Voltage at Maximum Power Point (*Vmp*)	29.6 V
Current at Maximum Power Point (*Imp*)	8.28 A
Short-Circuit Current (*Icc*)	8.83 A
Open-Circuit Voltage (*Vco*)	37.5 V
Temperature Coefficient of Voltage Sensitivity	-0.42 V/K
Temperature Coefficient of Current Sensitivity	+0,05 A/K

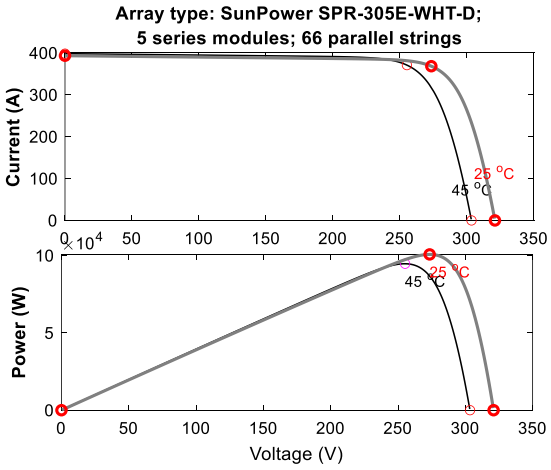

Fig. 1. The output characteristic curves of the PV array under variable conditions power-voltage curves; current-voltage curves

2.2. Boost converter modelling

The PV array is connected to a DC link capacitor via a DC-DC boost converter. The dynamics related to the PV array output voltage V_{pv} and the average current I_l flowing through the boost converter inductor can be written as follows. The DC Converter operates in both ON and OFF modes. In ON mode, as shown in Figure 2 current flows through the switch and the rest of the circuit are disconnected [26]. When the switch conducts (Switch ON State Figure 2b), the diode becomes reverse-biased, yielding the following dynamics:

$$\frac{dI_L}{dt} = \frac{1}{L}\left(V_{pv} - V_c\right) \tag{2}$$

$$\frac{dV_c}{dt} = \frac{1}{C}\left(I_c - \frac{V_c}{R} - I_c\right) \tag{3}$$

Where I_L is the inductor current, V_c the capacitor voltage, V_{pv} the PV source voltage, and R the load resistance. During this phase, the inductor stores energy while the capacitor discharges to the load. During switch turn-off (Figure 2a), the diode conducts, connecting the inductor to the output circuit:

$$\frac{dI_L}{dt} = \frac{1}{L}V_{pv} \tag{4}$$

$$\frac{dV_c}{dt} = -\frac{1}{RC}V_c - \frac{1}{C}I_c \tag{5}$$

Here, the inductor releases stored energy to both the capacitor and load, with the capacitor current I_c now influencing the voltage dynamics [27].

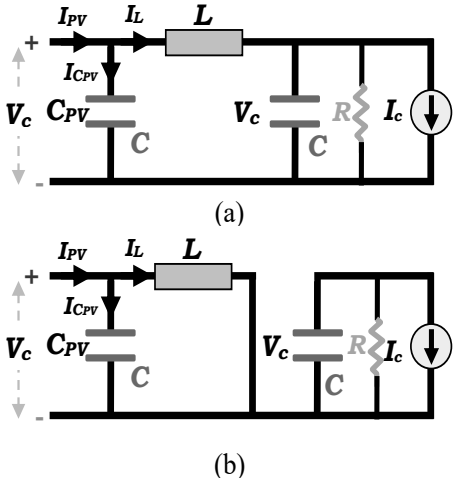

Fig. 2. Boost converter equivalent circuits: (a) switch OFF, (b) switch ON

$\bar{D} = [1 - D] \quad D\epsilon[0,1]$. Is the duty ratio of the switching signal to the power switch in the boost converter.

2.3. Voltage source converter (VSC) modelling and grid integration

The VSC is tasked with converting the DC output from the boost converter into AC power synchronized with the utility grid. To enhance simulation efficiency while retaining key dynamics, we adopt a simplified average model of the VSC. This converter is governed by a dedicated controller that ensures output voltage regulation and grid synchronization. It manages critical variables including the output voltage $V_{abc,gen}$, input current $I_{abc,gen}$, and reference signals $V_{abc,ref}$ for controlling voltage magnitude, frequency, phase, and active power [28].

A transformer electrically isolates the system and matches its voltage level to grid requirements. In the simulation, a three-phase transformer links the low-frequency AC output of the converter to the main grid. Compliance with grid standards is achieved through a filtering stage typically an RL or LCL filter with a parallel capacitor that suppresses high-frequency harmonics from the switching process, yielding clean sinusoidal waveforms [29].

The PV system connects to a simulated utility grid capable of both importing and exporting power, enabling validation of synchronization and power injection capabilities under dynamic operating conditions.

VSC Average Model: The averaging model bypasses the actual switching (PWM) and focuses on RMS or dq values: in the dqrotary frame (with the help of a PLL):

$$V_{dq,inv} = V_{dq,grid} + L\frac{di_{dq}}{dt} + Ri_{dq} + Lwi \tag{6}$$

Where $V_{dq,inv}$ Inverter voltage, $V_{dq,grid}$ Grid voltage, i_{dq} The current injected into the network, R, L The resistance and inductance of the bonding filter, the angular velocity is defined as: $w = f2\pi$.

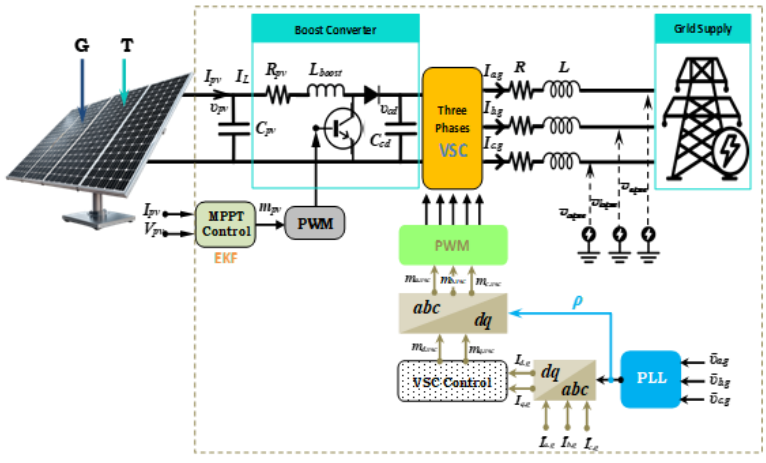

Fig. 3. Schematic Diagram of a PV based power system

Calculating active and reactive power is necessary in order to evaluate the performance of the photovoltaic system and monitor the effectiveness of the control strategy in different operating conditions.

$$P = \frac{3}{2}(i_d v_d + i_q v_q) \quad (7)$$

$$Q = \frac{3}{2}(i_q v_d - i_d v_q) \quad (8)$$

distance of the bonding filter, $w = f2\pi$ Angular velocity.

2.3.1. Transformer model

The transformer equation shown (Ep.9) represents the fundamental relationship in an ideal three-phase transformer connecting the voltage source converter (VSC) to the grid:

$$\vec{V}_{grid} = \vec{V}_{inv}., n \to n = \frac{\vec{V}_{grid}}{\vec{V}_{inv}} \quad (9)$$

Where n is the turns ratio, and $\vec{V}_{grid}$, $\vec{V}_{inv}$ represent grid- and inverter-side voltage vectors, respectively. The transformer ensures voltage matching, galvanic isolation, and harmonic attenuation. RL filter dynamics: The current di_{abc} between the VSC and grid is modeled as:

$$\frac{di_{abc}}{dt} \mathrm{L} + \mathrm{R} i_{abc} = V_{abc,grid} - V_{abc,inv} \quad (10)$$

Here, L and R denote the filter inductance (combining transformer leakage and added inductance) and resistance, critical for limiting *di/dt* transients and suppressing high frequency switching harmonics.

Grid synchronization: A PLL extracts the grid angle $\theta(t)$ for reference frame transformations ($abc \leftrightarrow dq$):

$$\theta(t) = \int_o^\tau \omega(\tau) d\tau \, , \theta = \omega \, , \theta_{grid} = \omega_{grid} \quad (11)$$

The PLL enables decoupled active/reactive power control in the synchronous dq frame and ensures frequency stability during grid disturbances. For weak grids, advanced PLL designs mitigate synchronization instability risks.

2.4. Estimation with an extended Kalman filter

In solar PV systems, real-time estimation of internal states such as voltage, current, temperature, and irradiance is vital for optimal performance and fault detection. Given the system's nonlinear nature, the (EKF) is employed as an effective estimation method. Unlike the classical Kalman Filter (KF), the EKF handles nonlinearity through linearization at each step. The EKF operates in two main phases:

- Prediction Step: Estimates the next state based on the nonlinear system model (previous differential equations).
- Correction Step: Adjusts the predicted state using actual measurements and their deviation from predictions.

The filter also incorporates model and measurement noise through process and observation noise covariance matrices.

3. IMPACT OF SENSOR MALFUNCTIONS ON PV SYSTEM PERFORMANCE

Sensors play a pivotal role in the operation of photovoltaic (PV) systems, facilitating real-time monitoring and optimization of energy production. They provide critical data on parameters such as irradiance, temperature, and solar incidence angle each essential for fine-tuning system operations and enhancing overall energy efficiency.

Malfunctions in these sensors can lead to inaccurate measurements, thereby compromising energy management strategies and degrading system performance. Consequently, assessing the influence of sensor faults on PV system behaviour is crucial for devising robust mitigation techniques. For instance, precise solar irradiance data is required for effective energy generation and grid integration. However, the fault diagnosis strategy in this study specifically focuses on electrical sensors, namely the voltage and current sensors located at the output of the photovoltaic (PV) array. These sensors provide the measured signals V_{pv} and I_{pv} , which are used for power assessment and as inputs to the EKF-based fault detection and correction scheme. The fault diagnosis framework focuses on voltage and current sensors at the PV array output, while sensors in the boost converter and transformer are not considered. By embedding this sensor data into advanced energy management frameworks, operators can enhance performance and extend system lifespan. In real-world PV deployments, the accurate measurement of current and voltage is vital for effective monitoring, control, and fault detection. Nevertheless, sensor readings are prone to multiple error sources, including random noise, systematic bias, and temporal drift. These inaccuracies can adversely affect model-based estimation and diagnostic algorithms, such as the (EKF). To enhance system resilience, it is imperative to construct dynamic models that explicitly characterize the nature of sensor faults. A sensor fault occurs when the measured value deviates from the true value due to calibration errors, noise, or drift over time. These deviations can be mathematically expressed using differential equations that capture their evolution:

$$y_{meas} = y_{true} + b + w(t) \quad (13)$$

Where: y_{meas} is the sensor-measured value (voltage or current), y_{true} is the actual value, b denotes the constant sensor bias, and $w(t)$ represents time-dependent random noise. The errors in the voltage and current sensor can be described by two equations:

$$y_{V\_meas} = y_{V\_true} + b_V + w_V(t) \quad (14)$$

$$y_{I\_meas} = y_{I\_true} + b_I + w_I(t) \quad (15)$$

Figure 4 shows the block diagram representing the flow of information from the true values. y_{V_true} and y_{I_true},through two error-generation pathways. Each signal is subject to an additive bias (b_V or b_I), This is followed by the addition of time varying noise ($w_V(t)$ or $w_I(t)$). This results in the

final measured outputs y_{V_meas} and y_{I_meas}, respectively. This modular structure enables each fault component to be isolated and analysed separately, improving diagnostic precision.

Relevance to Fault Detection and Estimation Accurate modelling of sensor faults is foundational to the development of robust state estimators and fault detection algorithms. By explicitly integrating bias and noise into the measurement model, observers such as the EKF can concurrently estimate physical states and sensor faults. This dual estimation capability improves overall accuracy and facilitates early detection of sensor degradation or failure. The inputs y_{V_true} and y_{I_true} correspond to the true voltage and current generated by the PV array before being affected by sensor faults.

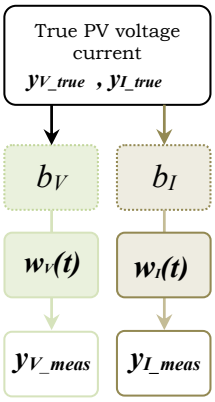

Fig. 4. Schematic diagram of the dynamic modelling of sensor faults in PV measurement systems

Integrating the sensor fault model within the EKF framework enables real-time estimation of both system states and sensor errors without necessitating additional hardware. This approach supports a streamlined, accurate diagnostic mechanism that boosts fault tolerance and enhances the reliability of state estimation.

In Figure 5, the Extended Kalman Filter is a mathematical algorithm used to estimate the true state of a system when measurements are inaccurate or subject to noise. In this context, it estimates the true voltage ($\hat{V}_{PV}$) and current ($\hat{I}_{PV}$) of the solar cell. And The Maximum Power Point Tracking (MPPT) algorithm is designed to extract the maximum power possible from a solar cell. It takes the control signal output from the MPPT and converts it to a PWM (Pulse Width Modulation) signal. This signal controls the electronic switch (ST) in the Boost DC-DC converter, which increases the voltage output from the solar cell. The ST switch is controlled by the PWM switch, which is switched on and off at high speed. The design of this converter allows the voltage to be adjusted to meet load requirements. In the presence of sensor malfunctions, deviations are introduced into the measured signals, leading to inaccurate and unreliable measurements. These faults can propagate through the control units and significantly degrade the overall performance of the photovoltaic system.

In particular, errors affecting the voltage and current sensors result in corrupted measurements of the photovoltaic array, denoted as $\tilde{V}_{pv}$ and $\tilde{I}_{pv}$ Such measurement faults may arise from sensor degradation, bias, or noise, and can adversely impact the efficiency of the MPPT algorithm and the stability of the system. where $\tilde{V}_{pv}$ and $\tilde{I}_{pv}$ represent the corrupted voltage and current measurements affected by sensor faults, while V_{pv} and I_{pv} denote the true values of the photovoltaic system. The MPPT algorithm in photovoltaic systems uses the estimated values $\hat{V}_{pv}$ and $\hat{I}_{pv}$ to determine the optimal duty cycle D_{MPP} ,ensuring maximum power extraction under varying operating conditions. The MPPT algorithm determines the optimal duty cycle based on the estimated voltage and current, which can be expressed as:

$$D_{MPP} = f(\hat{V}_{pv}, \hat{I}_{pv}) \tag{16}$$

However, in the presence of measurement errors and sensor faults, the MPPT may operate at a non-optimal point, leading to reduced energy extraction. In this case, the operating duty cycle deviates from its optimal value, i.e ($D \neq D_{MPP}$, $P_{pv} \neq P_{pv,MPP}$) which results in a degradation of the overall photovoltaic system performance.

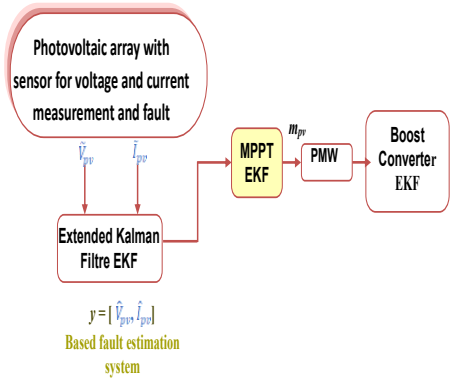

Fig. 5. EKF-based estimation and control architecture for sensor fault mitigation and maximum power point tracking (MPPT) in photovoltaic (PV) systems

The integration of estimation, fault diagnosis, and control within a unified EKF-based framework significantly enhances the reliability of PV systems. It enables the detection of sensor faults through continuous deviation tracking, improves MPPT efficiency by utilizing corrected measurements, and strengthens overall system robustness. By minimizing the influence of erroneous readings, this integrated approach mitigates performance degradation and reduces the risk of system-level failures.

4. EKF-BASED FAULT DIAGNOSIS FOR PHOTOVOLTAIC SYSTEMS

This work proposes a fault diagnosis system for photovoltaic (PV) systems based on the (EKF). The primary objectives of the system are to:

- Estimate the true values of the PV output voltage (V_{pv}) and current (I_{pv}) using EKF.
- Detect sensor faults by analysing the residuals between measured and estimated values.
- Detect sensor faults and infer their characteristics through residual-based threshold analysis.
- Replace faulty sensor data with corrected values to maintain reliable control, particularly in (MPPT) operations.

Maximum power point tracking (MPPT) operations. Figure 6 presents the architecture of the proposed fault-tolerant estimation and sensor validation strategy for PV systems, which is grounded in a model-based estimation framework using the EKF.

This approach integrates dynamic modelling, residual generation, fault detection logic, and intelligent switching to achieve robust system performance under sensor fault conditions.

The process begins with a nonlinear dynamic model of the PV panel that simulates voltage and current outputs as functions of solar irradiance (G) and temperature (T). These simulated outputs are then processed by a sensor block, which mimics real world measurements that may be affected by various types of sensor faults, such as bias, random noise, or drift. The resulting measured signals serve as inputs to both the estimation and diagnostic modules.

At the core of the system, the Extended Kalman Filter uses the nonlinear PV model in conjunction with real-time irradiance and temperature data to estimate the actual output voltage ($\tilde{V}_{pv}$) and current ($\tilde{I}_{pv}$). The EKF continuously refines its estimates by minimizing prediction errors through recursive updates based on incoming measurements. The discrepancies between estimated and measured values termed residuals are calculated as follows:

$$\begin{cases} v_r = \tilde{V}_{pv} - \hat{V}_{pv} \\ i_r \ = \tilde{I}_{pv} - \hat{I}_{pv} \end{cases} \tag{17}$$

These residuals are then evaluated against predefined thresholds using a comparator. If either residual exceeds its corresponding threshold whether static or adaptively tuned a fault is flagged.

To enhance diagnostic reliability and suppress the influence of transient noise, the residuals are processed by a fault detection logic module. This block may employ techniques such as thresholding with moving average (MA) filters to isolate persistent anomalies from random fluctuations. A fault-tolerant switching mechanism is implemented to select the most reliable signals based on filtered residuals and validated fault detection logic. This logic determines whether the control unit should rely on the original measured values or switch to the EKF-estimated values. If the sensor is deemed reliable, the measured signal is retained; otherwise, the system defaults to the EKF estimate to ensure uninterrupted and accurate MPPT operation.

The figure 6 illustrates the proposed fault-tolerant maximum power point tracking (MPPT) strategy for photovoltaic (PV) systems based on an Extended Kalman Filter (EKF). First, the PV voltage and current are measured through the sensor block, generating the signals V_{pv}^{used} and I_{pv}^{used} which may be affected by noise or sensor faults.

These measurements are then processed by the EKF, which uses the nonlinear PV model along with environmental inputs such as irradiance G and temperature T to estimate the system states $(\hat{V}_{PV}, \hat{I}_{PV})$. Finally, the selected signals $(V_{pv}^{used}, I_{pv}^{used})$ are fed into the MPPT controller of the boost converter, ensuring accurate tracking of the maximum power point even under sensor fault conditions.

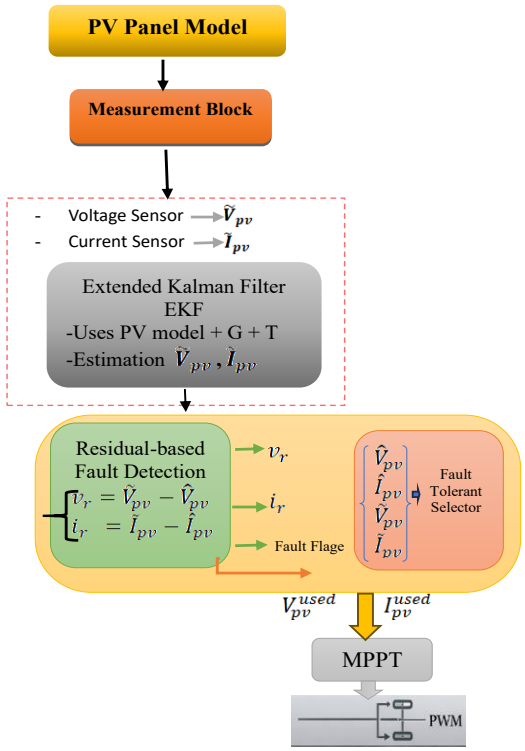

Fig. 6. Proposed EKF-based fault-tolerant MPPT control scheme for PV systems using residual-based sensor fault detection

4.1. Desings of Extended Kalman Filter EKF

EKF is a very useful tool that can be used to estimate the state or parameters in many engineering problems. This tool is based on the discrete non-linear model of the system. The (EKF) is a specialized version for non-linear systems [30]. It estimates the true state of the system (voltage and current) based on noisy measurements [31]. The (EKF) is a modified version of the original Kalman filter, designed for nonlinear systems. The Kalman filter (KF) is used only for linear systems. The EKF approximates a nonlinear system to a linear one using first-order Taylor derivatives (Jacobians). In the following, the design procedure of the EKF is presented in detail.

Algorithm An Extended Kalman Filer for State Estimation

Inputs:

x_0: Initial state estimate.
P_0 : initial error
Covariance matrix. Q : process noise covariance
Covariance matrix R: measurement noise covariance matrix, and z_k : measurement vector at time k.

Initialization:

- Set $x_{0|0} = x_0$
- Set $P_{0|0} = P_0$

Processing:

For each time step k from 1 to N, do:

1. Prediction Step

State Prediction:

$$f(x_{k-1}) = x_{k|k-1} \tag{18}$$

$$x_{k-1} = x_{k|k-1} \rightarrow x = f(x) \tag{19}$$

Covariance Prediction:

$$P_{k|k-1} = Q + A^T P_{k-1} A \tag{20}$$

Where: $A_x = \frac{\partial f}{\partial x}\Big|_{x=k-1}$ Derivative of the model (here the identity matrix $A = I$)($k-1$ Jacobian of f at x).

2.Measurement Prediction:

Predicted Measurement Using Nonlinear Model:

$$I_{pv\_model} = I_{sc} - I_o\left(exp\left(\frac{q(V_{pv}-I_{pv})}{nkT}\right) - 1\right) \tag{21}$$

Construct Measurement Vector:

$$z_{pred} = \begin{bmatrix} V_{pv} \\ I_{pv\_model} \end{bmatrix} \tag{22}$$

3. Update Step:

Measurement Residual:

$$y_k = z_{pred} - z_k \tag{23}$$

Compute Measurement Jacobian:

$$H_k = \frac{\partial h}{\partial x}\Big|_{x=k-1|k} \tag{24}$$

Kalman gain:

$$K_k = P_{k|k-1} H_k' * inv\left(H_k P_{k|k-1} H_k' + R\right) \tag{25}$$

4. Correction Step:

State Update:

$$X_{k|k} = x_{k|k-1} + K_k + y_k \tag{26}$$

$$P_{k|k} = P_{k|k-1}(H_k * K_k - I). \tag{27}$$

End

d. Outputs:

Updated state estimate $x_{k|k}$
Updated covariance matrix $P_{k|k}$

Initially, the following initial values are determined, and the future state is predicted based on the mathematical model of the solar panel. A nonlinear model is used to calculate the expected values of the measurements, as seen in (21). The nonlinear model is similar to the current equation in the solar cell. The measurement is then predicted, and the estimates are corrected using the actual measurements in (23) and (24), thus correcting the state and correcting the variance in (25) and (26). The purpose of the EKF in a PV system:

- Compensating for sensor failures.
- Improving the accuracy of instantaneous estimation.
- Porting the MPPT algorithm through reliable estimations.

This work also presents, as shown in Figure 5, a discrete-time modelling approach for boost converter dynamics and designs an (EKF) for accurate state estimation. The system considers both switch ON/OFF states, derives discrete-time equations using forward Euler discretization, and implements an EKF to estimate inductor current, output voltage, and load current under measurement noise and system uncertainties.

Algorithm B Boost Converter State Estimation via Extended Kalman Filter

Inputs:

- System Model: Continuous-time matrices $\boldsymbol{A}, \boldsymbol{B}, \boldsymbol{C}$ (defined below), and Sampling time T_s.
- Initial Conditions: $x_0 = \left[I_{pv}(0), V_c(0), I_0(0)\right]^T$ (initial state vector), and P_0 (initial covariance matrix).
- Noise Covariances: $\boldsymbol{Q}$ (process noise), and $\boldsymbol{R}$ (measurement noise).
- Measurements: $y_k = [V_c(k), I_0(k)]^T$ (measured outputs), and $u_k = \left[V_{pv}(k), I_0(k)\right]^T$ (known inputs)

Initialization:

- Set initial state estimate: $\hat{x} = x_0$
- Set initial covariance: $P_{0|0} = P_0$ given initial uncertainty

Processing:

For each time step k from 1 to N, do:

1. Prediction Step

State Prediction:

$$\hat{x}_k = A_d \hat{x}_{k-1} + B_d u_{k-1} \tag{28}$$

Where

$$\mathrm{A_d} = \mathrm{I} + \mathrm{T_s A}\text{ , and } \mathrm{B_d} = \mathrm{T_s B} \tag{29}$$

$$A = \begin{bmatrix} 0 & \frac{-1-S}{L} & 0 \\ \frac{Rs-s}{RpC} & \frac{-1}{RC} & 0 \\ 0 & 0 & 0 \end{bmatrix},\ B = \begin{bmatrix} \frac{1}{L} & 0 \\ 0 & \frac{-1}{C} \\ 0 & 0 \end{bmatrix} \tag{30}$$

Covariance Prediction:

$$\mathrm{P_{k|k-1}} = \mathrm{Q} + \mathrm{F_{k-1}^T P_{k-1} F_{k-1}} \tag{31}$$

Where: $F = \frac{\partial}{\partial x}(A_d x_k + B_d u_k)_{\hat{x}_k}$ (Jacobian)

2. Kalman Gain Calculation:

$$K_k = \bar{P}_k C d^T (C_d \bar{P}_k {C_d}^T + R)^{-1} \tag{32}$$

Where: $C_d = C = \begin{bmatrix} 1 & 0 & 0 \\ 0 & 0 & 1 \end{bmatrix}$.

3. Correction Step:

State Update:

$$\hat{x}_k = \hat{x}_k^- + K_k(y_k - C_d\, \hat{x}_k^-) \tag{33}$$

Covariance Update:

$$P_k = \bar{P}_k - K_k C_d \bar{P}_k \tag{34}$$

4. Go back to step 2

End

d. Outputs:

Estimated states: $\hat{x}_k = \left[\hat{I}_{pv}(k), \hat{V}_c(k), \hat{I}_0(k)\right]^T$

Maximum Power Point Tracking (MPPT) is essential in photovoltaic (PV) systems to ensure optimal energy extraction under varying environmental conditions. Traditional MPPT methods, such as Perturb and Observe (P&O) and Incremental Conductance (INC), suffer from oscillations around the maximum power point (MPP) and slow convergence under rapidly changing irradiance. To address these limitations, this work proposes an (EKF)-based MPPT algorithm, which combines the robustness of stochastic estimation with the dynamic tracking capability of recursive filtering.

The state variable is the PV voltage, denoted as v_k, at the (MPP), and its objective is to estimate the true MPP voltage despite measurement noise and system nonlinearities. Key advantages include slope-aided prediction, where the algorithm leverages the local slope of the P-V curve (dP/dV) to predict the MPP voltage, along with noise immunity, since process noise (Q) and measurement noise (R) covariances are explicitly modelled to improve robustness and recursive efficiency, since the filter updates its estimates in real-time with minimal computational overhead.

Algorithm C Extended Kalman Filter for MPPT Tracking

Inputs:

- v_k, I_k: Measured PV voltage and current (real numbers).
- v_{out}: Converter output voltage (real number).
- **Q**, **R**: Process and measurement noise covariances (default: 50).
- Step: Perturbation step size (default: 5).
- System Model:

$$v_k = Av_{k-1} + B\left(\frac{dP}{dV}\right)_{k-1} + w_k \tag{35}$$

Where: v_k= PV voltage at step k.

$A = 1$ (state transition matrix).

$B = \Delta t$ (step size, typically 5).

$\left(\frac{dP}{dV}\right)_{k-1} = \frac{P_k - P_{k-1}}{v_k - v_{k-1}}$ (PV curve slope).

$w_k = \sim\mathcal{N}(0, R)$ (Process noise).

Measurement equation:

$$z_k = Cv_k + \mathcal{U}_k \tag{36}$$

Where: z_k : measured PV voltage.

$C = 1$ (Observation matrix).

$u_k = \sim\mathcal{N}(0, R)$ (Measurement noise).

Initialization:

- Set initial state estimate: $\hat{x} = x_0$
- Set initial covariance: $\hat{P}_k = P_0$ given initial uncertainty

Processing:

For each time step k from 1 to N, do:

1. Prediction Step

Predicted state estimate:

$$\hat{v}_k^- = \hat{v}_{k-1} + B\left(\frac{dP}{dV}\right)_{k-1} \tag{37}$$

Predicted error covariance:

$$P_k^- = P_{k-1} + Q \tag{38}$$

2. Update Step (Measurement Update)

Kalman gain:

$$K_k = \frac{P_k^-}{P_k^- + R} \tag{39}$$

Updated state estimate:

$$\hat{v}_k = \hat{v}_k^- + K_k(z_k - \hat{v}_k^-) \tag{40}$$

Updated error covariance:

$$P_k = (1 - K_k)P_k^- \tag{41}$$

End

d. Outputs:

Duty Cycle Calculation:

$$D_{MPP} = 1 - \frac{\hat{v}_k}{V_{out}} \tag{42}$$

Where V_{out} is the converter output voltage.

The (EKF) for MPPT recursively predicts and corrects system dynamics, starting with state prediction in (37), where $B = \Delta t$ represents step size and dP/dV is the instantaneous slope of the P-V curve. In parallel, the error covariance P_k^- changes based on (38), where Q represents process noise and model uncertainty. The filter updates (39) with real-time data z_k, optimizing prediction against measurement noise covariance R with Kalman gain. The state estimate $\hat{v}_k$ directly affects the duty cycle D_{MPP} (42) of the power converter, ensuring optimal performance despite ambient circumstances and measurement noise. This closed-loop energy harvesting method combines model-based prediction and sensor feedback for robustness and efficiency.

5. FAULT DETECTION AND DIAGNOSIS

5.1. Residual calculation

After performing the estimation phase using the (EKF), the quality of the estimate can be assessed by comparing the actual measured values with the values estimated by the filter. This is done by calculating the residuals, which are the differences between the actual measurements and the estimates in (17).

The residual signals are constructed based on the difference between the measured outputs and the EKF-estimated states. The EKF relies on the nonlinear PV model described in (1) and the measurement equations in (17) to generate estimates of the PV voltage and current. These estimates are then used to compute the residuals in (17), which serve as fault indicators for the detection scheme.

5.2. Adaptive threshold

The standard deviation of the residuals is used to determine dynamic thresholds for defect detection, Threshold Definition:

Th_{1v} , Th_{2i}: Thresholds to be determined (fixed or adaptive).

If $(|r_v| > Th_{1v} \ \ or |r_i| > Th_{2i})$ a fault is declared. These thresholds can be computed as:

$Th_{1v} = \alpha.\sigma_{rv}$, $Th_{2i} = \alpha.\sigma_{ri}$ Where:

- σ_{rv}, σ_{ri}: Standard deviations of the voltage and current residuals under normal operation.

- α: A tuning coefficient controlling sensitivity.

The coefficient α is selected based on statistical considerations and empirical tuning in order to balance the sensitivity and robustness of fault detection against noise. Increasing the value of α has two effects. Firstly, it reduces false alarms. However, it can also delay fault detection. On the other hand, decreasing the value of α increases sensitivity. However, this comes at the expense of robustness.

- Compared to fixed thresholds, this adaptive method improves detection reliability by accounting for system noise fluctuations and reducing false alarms.
- They can be calculated using the moving average or standard deviation of the normal operating variables. This method automatically adapts to noise changes in the system and minimizes the errors caused by using a fixed threshold.

5.3. Intelligent switching

When a sensor malfunction is detected: Signal Replacement: The measured value from the faulty sensor is replaced by the estimated value from the (EKF) in the control system to ensure continuity of operation.

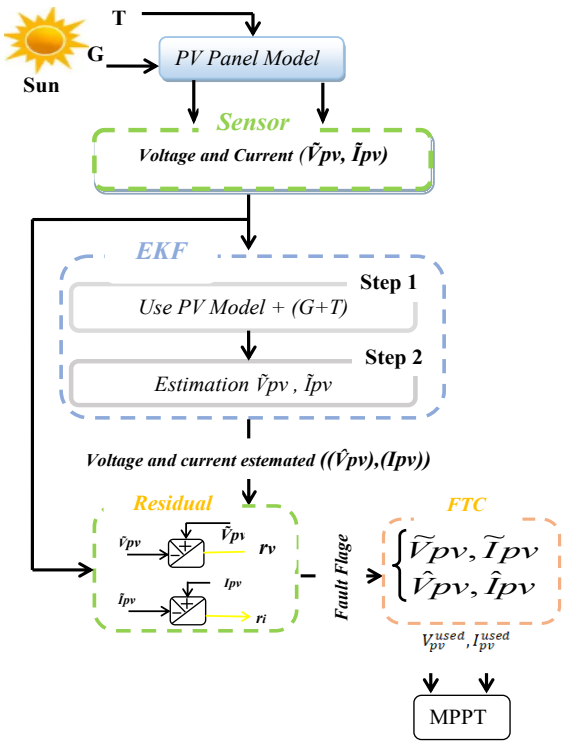

Fig. 7. Proposed strategy for mitigating faults in PV output voltage and current sensors

5.4. Event logging

Event logging is a critical component of fault detection systems, especially those employing an estimation-based approach, such as the (EKF). When a sensor fault is detected, an automatic logging mechanism records detailed information relating to the fault. This enables real-time alerts, preventive maintenance, and post-event analysis.

Event log content: Each fault event is documented with the following information:

- Timestamp: Records the exact time of the fault occurrence, enabling correlation with system operating conditions or external factors.
- Sensor type affected: Identifies the faulty sensor (e.g. voltage or current sensor), helping to locate the source of the fault.
- Replaced value: The value estimated by the EKF to replace the unreliable measurement from the faulty sensor.

5.5. RMS Assessment before and after diagnostic implementation

The RMS value is a key metric for assessing the magnitude of a varying signal. This is particularly important in the analysis of electrical signals, where it serves as a reliable indicator of distortion or deviation from expected values. In the context of fault detection and diagnosis (FDD), quantifying the effectiveness of the fault mitigation approach involves evaluating the RMS values before and after applying a diagnostic strategy.

To calculate the RMS of a discrete-time signal $x(i)$ over N samples, the following formula is used:

$$RMS = \sqrt{{}^{2}_{i}x \sum_{i=1}^{N} \frac{1}{N}} \tag{43}$$

Equation calculates the square root of the mean of the signal's instantaneous values squared. This makes it sensitive to variations in both amplitude and frequency, effectively capturing the signal's energy content. In our analysis, we apply this metric to the voltage and current signals from the photovoltaic (PV) system under study. By calculating the (RMS) error between the true (or reference) signal and the measured signal, we can evaluate the extent of deviation caused by sensor faults.

Before diagnosis: The RMS error is typically high due to faults such as sensor bias, drift, or noise, which distort true system measurements.

After diagnosis: Once the proposed diagnostic strategy has been applied the RMS error is expected to decrease significantly. This indicates that faults have been successfully compensated for and the original signal behaviour recovered. This reduction in RMS error is a key quantitative performance indicator, demonstrating the capability of the diagnostic method to restore the integrity of the system's measurements. In practical terms, a lower RMS value after diagnosis implies more accurate and reliable system operation, which is essential for control and optimization in applications such as renewable energy systems.

Figure 8 illustrates the residual-based fault detection mechanism integrated with the (EKF) for monitoring PV sensor measurements. The process begins with the acquisition of the measured PV voltage and current signals, $(\tilde{V}_{pv}, \tilde{I}_{pv})$, which may be affected by sensor faults. These measurements are then processed by the EKF, which provides

estimated values $\hat{V}_{pv}$ and $\hat{I}_{pv}$ based on the nonlinear PV model. The residuals are computed as the difference between the measured and estimated signals, i.e., r_v , r_i. These residuals are evaluated using a threshold-based decision logic, where a fault is declared when the magnitude of the residual exceeds a predefined threshold. An alert is sent to the maintenance team. The data is stored for later analysis and reporting purposes

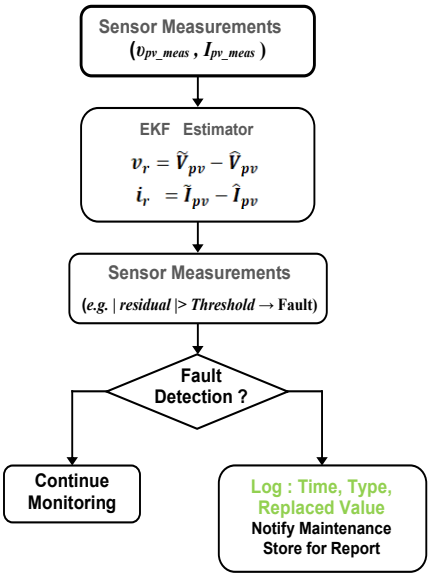

Fig. 8. This is a process flowchart for detecting and recording sensor failures using threshold estimation and comparison

6 SIMULATION RESULTS / DISCUSSION

In order to evaluate the effectiveness of the proposed diagnostic approach in enhancing the resilience of photovoltaic (PV) systems in the event of sensor faults, detailed simulation studies were carried out. This section presents a comparative analysis of three operating scenarios: (i) normal operation without faults; (ii) faulty operation with no diagnostic mechanism; and (iii) fault-tolerant operation using the proposed (EKF)-based framework.

Figure 9 presents the time-varying profiles of solar irradiance and ambient temperature used in the simulations. Solar irradiance (G) in W/m² Initially (up to approximately 0.1 seconds): The irradiance value remained constant at 500 W/m². From 0.1 to 0.2 seconds: The value increased to 1000 W/m². From 0.2 to 0.25 seconds: It decreased to 800 W/m². After that, it stabilized again at 600 W/m². The temperature is approximately 20°C.After approximately 0.1 seconds, it gradually rises to 22°C. Then it increases to 24°C after around 0.2 seconds. It finally stabilizes at 25°C after approximately 0.25 seconds.

6.1. Study of the behaviour of a healthy PV system in the absence of sensor faults

The performance of the photovoltaic (PV) system is examined in the absence of faults or sensor deviations, such as those affecting the voltage and current sensors. This study will be used as a baseline for comparing performance results in the presence of faults.

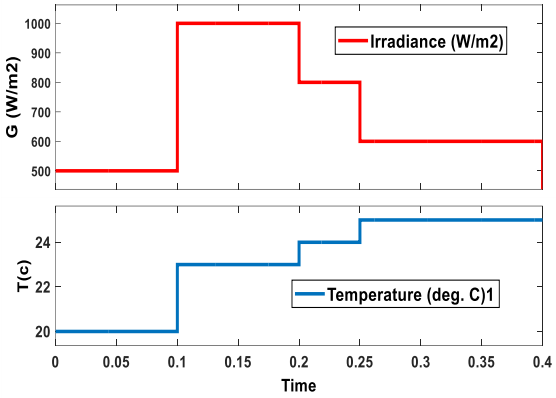

Fig. 9. Solar radiation and temperature change over time

Establish a baseline for the photovoltaic system, ensuring there is no interference or measurement error. Verify the accuracy of the PV model and control units, such as the maximum power point tracker (MPPT). Record real signals for later comparison with cases where errors occur. Calculate performance metrics such as RMS error and MPPT efficiency. The voltage and current readings are smooth and consistent with the weather conditions. The MPPT efficiency is close to 100%.

The results presented in Figure 10(a,b,c) are obtained through simulation. The PV voltage and current are generated using a nonlinear PV model under varying irradiance and temperature conditions, as defined in Figure 10. Sensor faults are artificially introduced into the measured signals to evaluate the effectiveness of the proposed EKF-based fault detection and mitigation strategy.

This scenario serves as a reference baseline for evaluating the effectiveness of the proposed diagnostic strategy. Although no estimation or correction is required in this case, the clean, stable signals establish the expected system behaviour under ideal conditions. These results enable a clear comparison with faulted scenarios, later demonstrating the utility of the EKF in restoring system stability.

- **Voltage (V_{PV}):** Stabilizes at ~200 V after transient fluctuations. Matches reference signal closely after 0.1 s, indicating effective inverter regulation.
- **Current (I_{PV}):** Oscillations in the first 0.05 s, followed by alignment with reference current. Control system tracks MPPT accurately.
- The system exhibits stable operation and optimal power extraction under ideal conditions.

Three-phase current (Iabc_B1) represents the three phase currents at point B1 of the network. Being equal in amplitude and frequency and phase-separated indicates that the system is in a healthy operating state. The initial oscillations are normal and disappear upon stabilization.

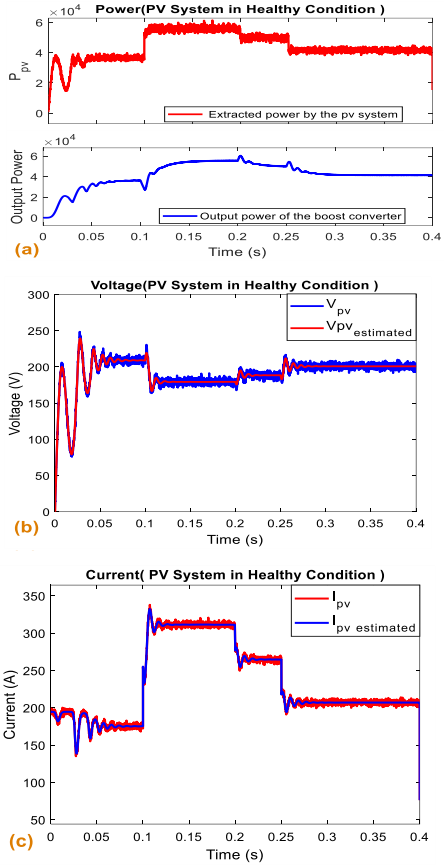

Fig. 10. PV System in Healthy Condition (Without Sensor): (a) Power, (b) Voltage, and (c) Current

Figure 14a: Three-phase Current (Iabc_B1). Iabc_B1:1, Iabc_B1:2 and Iabc_B1:3 (representing the three-phase currents). Observation The three waves are equal in amplitude and frequency and are phase separated (i.e., a balanced three-phase system). There are slight oscillations at the beginning (transient), followed by stabilization.

Figure 14b: Three-phase voltage (Vabc_B1). Vabc_B1:1, Vabc_B1:2 and Vabc_B1:3. Multiplied by 10^4 The maximum value is approximately 22,000 volts. The system is balanced, and the voltages are phase-separated and identical in shape. The frequency and amplitude are almost constant.

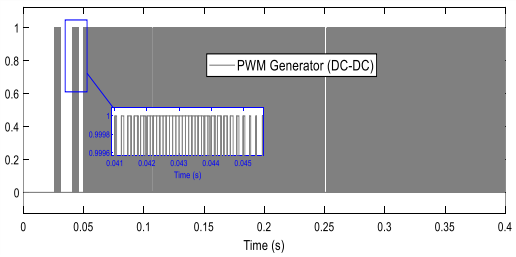

Fig. 13. PWM waveforms of proposed system

There are no signs of faulty sensors or imbalances in the system. The beginning of each figure shows the transient response, after which the system stabilizes in a steady state. here are oscillations at the start of operation (transient), after which it becomes stable.

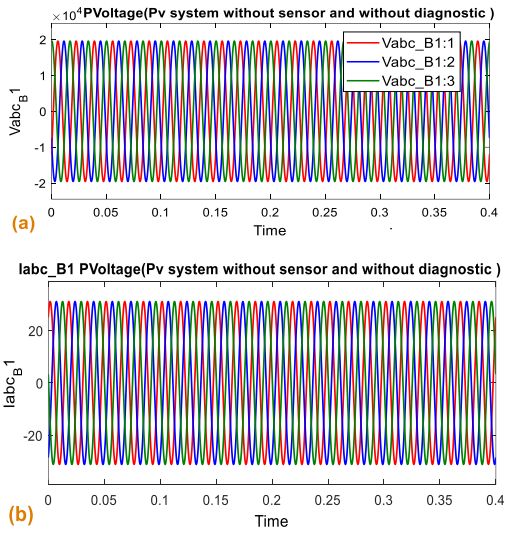

Fig. 14. Voltage and Current Waveforms Under Healthy PV System Operation Without Sensor Faults

6.2. Study of the behaviour of a photovoltaic system under sensor fault without diagnostic

Operating a solar power system (PV system) with a sensor fault (Sensor Fault) without a diagnostic strategy (Without Diagnostic Strategy) makes the system unreliable and significantly affects its performance. This makes the system inflexible, increasing the risk of failure or poor performance, particularly in grid-connected systems.

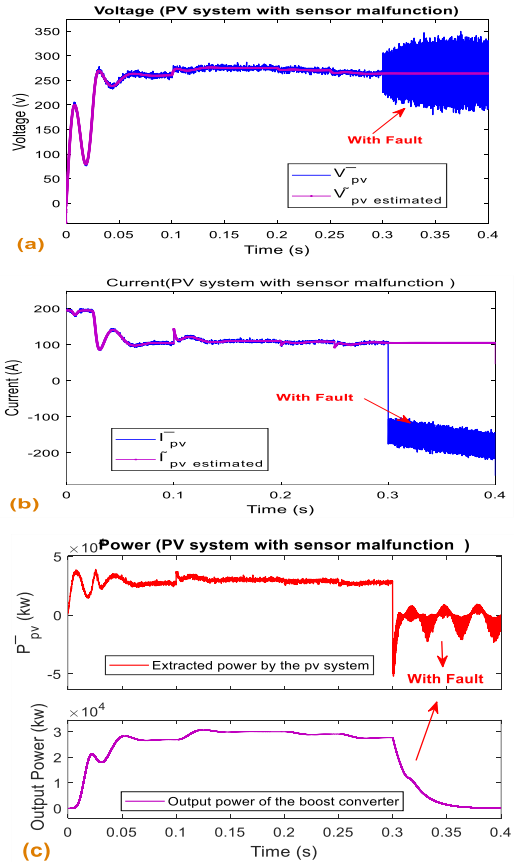

Fig.15. PV system operating with a sensor fault (no diagnostic applied): Voltage (a), Current (b), Power (c)

As shown in Figure 15 (a, b, c) the system performance under sensor fault conditions without any diagnostic strategy is significantly degraded. The control unit relies on corrupted voltage and current measurements, resulting in unstable power output and distorted MPPT operation.

Voltage behaviour (Figure 15a): Voltage with sensor fault without diagnostic). From 0 to ~0.3 s, the voltage remains stable at ~310–320 V, indicating normal operation. At t ≈ 0.3 s, the measured voltage (blue) becomes highly noisy and deviates from the true value (magenta). The zoomed inset clearly shows the wide deviation. Without a diagnostic strategy, the system continues to use the noisy signal, leading to instability in MPPT and system inefficiency.

Voltage sensor failure causes erroneous measurements that disrupt system control. Current behaviour (Figure 15b): current with sensor fault without diagnostic): initially, the current reaches ~60 A during startup, then stabilizes. At t ≈ 0.1 s, disturbances indicate intermittent sensor degradation.

At t ≈ 0.3 s, the measured current drops to zero, while the estimated (or actual) current exhibits high noise. The absence of diagnosis causes the controller to act on invalid measurements. A current sensor fault results in inaccurate feedback, which degrades control accuracy and risks converter malfunction. PV power shows an initial spike of up to ~40,000 W, followed by a sharp drop after 0.01 seconds. Eventually, PV power collapses to near zero due to reliance on faulty sensor data. Output power increases steadily to ~280,000 W and stabilises. The discrepancy between PV power and output power highlights the fact that the inverter is operating on unreliable data, which degrades MPPT performance. In the absence of a diagnostic system, there is a critical mismatch between the power generated and the power delivered, which undermines energy efficiency and system credibility.

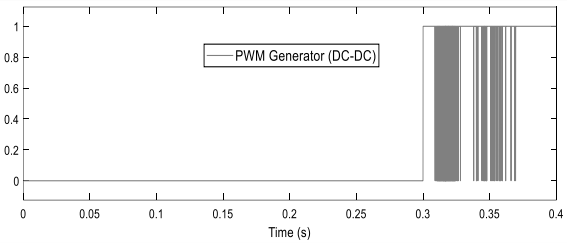

Fig. 16. PWM waveforms of proposed system

Current response (*Iabc_B1*): Initially, triple currents show unstable oscillations as a result of the fault but then stabilize as balanced sine waves. This suggests that, despite the absence of diagnostics, the system is attempting to maintain equilibrium.

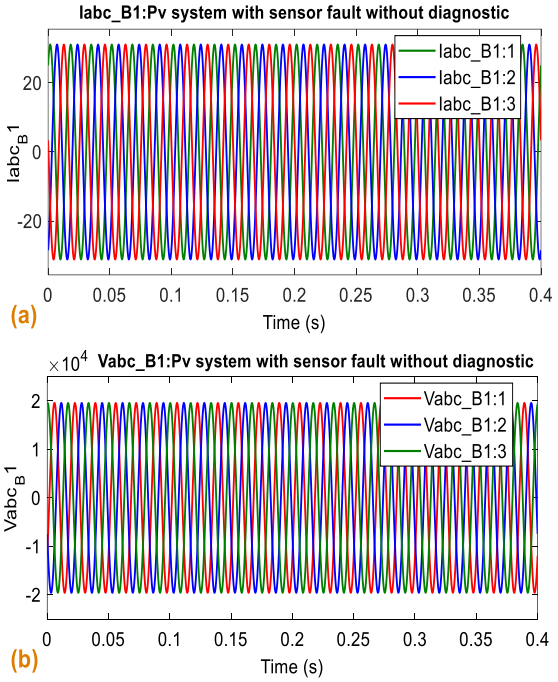

Fig. 17. Three-Phase Current Response (Iabc_B1) of the PV System under Sensor Fault Without Diagnosis(a), Three-Phase Voltage Response at the Point of Interconnection (Vabc_B1) under Sensor Fault Without Diagnosis (b)

Voltage response at the tie point (*Vabc_B1*): The voltages remain balanced and sinusoidal, which suggests that the inverter module is operating relatively stable at the voltage level despite the faulty sensor.

Inverter voltage (*Vab_VSC*): A sharp oscillation appears at the onset of the fault, gradually subsiding to become stable. This indicates that the system is attempting to correct its behaviour automatically despite the lack of a diagnostic mechanism. While the system appears to stabilize over time, an undetected fault can result in efficiency losses or component damage if not addressed promptly.

3.6. Study of the behaviour of a PV system under sensor malfunction with the proposed diagnostic strategy

This study analyses the performance of a PV system when a sensor malfunctions, but with a smart diagnostic strategy that aims to automatically detect and correct this malfunction. The objective of this study is to monitor the impact of sensor faults, such as deviation in V_{pv} or I_{pv}, on system performance. Apply an intelligent diagnostic strategy (such as EKF, Threshold-based FDI). Compare performance before and after diagnosis implementation. Demonstrate the effectiveness of the algorithm in restoring correct signals and improving system stability.

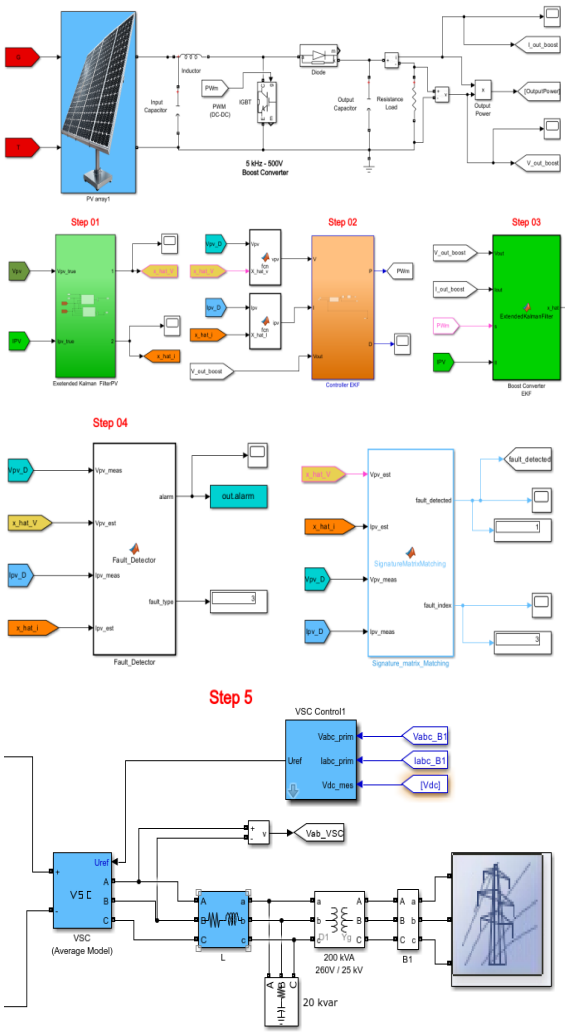

Fig. 18. Design and Simulation of PV based power system

Figure 19 (a, b, c) demonstrates the excellent performance of the proposed EKF-based fault-tolerant control strategy. Despite disturbances, the EKF accurately estimates true voltage and current in real-time. As a nonlinear intelligent observer, EKF detects discrepancies (residuals) between measured and predicted signals, and then feeds corrected data to the MPPT controller via a smart switching mechanism. The result is a stable, noise-free response, confirming EKF's ability to preserve performance even in fault conditions. This highlights its dual contribution as both an estimator and an embedded diagnostic tool ensuring robust fault tolerance.

Voltage behaviour (Figure 19a): Voltage with Sensor Fault and Proposed Diagnostic Strategy). Initially, the measured and estimated voltages align, indicating normal operation. At t ≈ 0.3 s, the measured voltage exhibits noise and deviation due to the simulated fault scenarios. The EKF-estimated signal, however, remains smooth and consistent throughout. A zoomed inset shows the significant discrepancy between the faulty measurement and the EKF correction. The controller detects this discrepancy and switches to the estimated signal, thereby maintaining control stability and voltage regulation.

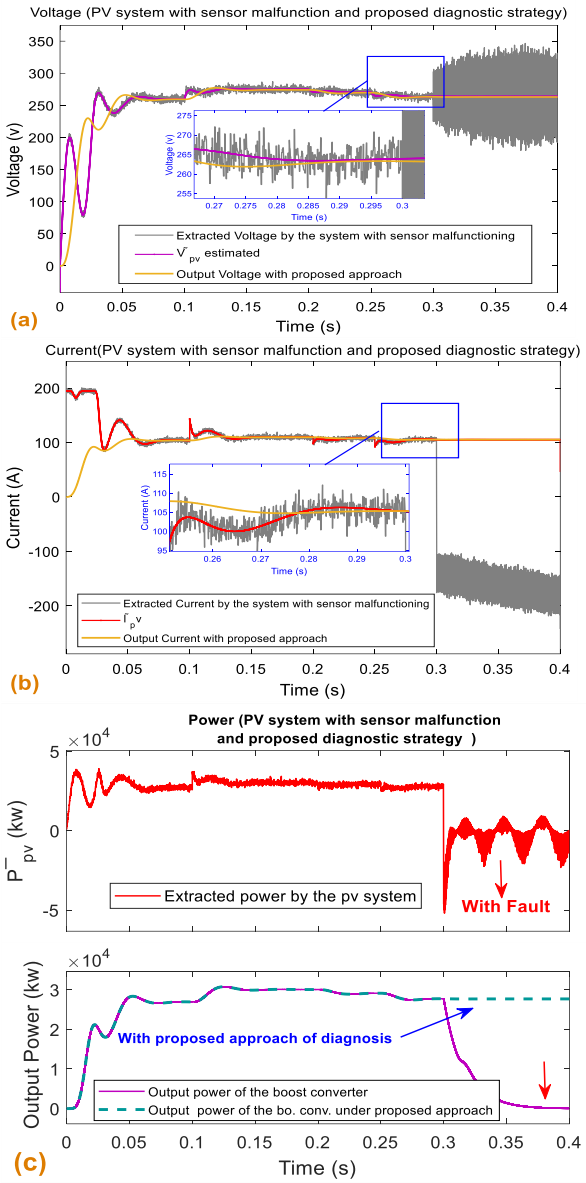

Fig. 19. (a) Voltage, (b) Current, Power (b), PV system with sensor malfunction and proposed diagnostic strategy

The observer-based diagnostic mechanism effectively mitigates the impact of voltage sensor faults, ensuring the continuity of maximum power point tracking (MPPT) and voltage balance.
Current Figure 19b: Current with Sensor Fault and Proposed Diagnostic Strategy). The measured current exhibits abrupt steps at t ≈ 0.1 s, 0.18 s and 0.25 s, as well as a clear collapse at t ≈ 0.3 s, which simulates different fault types. The estimated current remains stable throughout, reflecting robust estimation by EKF. The mismatch post-fault indicates that the diagnostic system has successfully switched to the estimated signal, enabling MPPT to function. The EKF-based strategy maintains current integrity and mitigates the effect of multiple sensor fault types.

Under sensor fault conditions, the PV power output as show in the Figure 19c, is subject to

noticeable disturbances due to inaccurate sensor readings. This is particularly evident in the form of sudden dips and irregularities in the PV power curve. Nevertheless, the application of the proposed diagnostic strategy enables the system to maintain relatively stable output power despite the sensor error. The corrective mechanism identifies and compensates for sensor anomalies, thereby preventing significant power loss or system instability. This demonstrates the robustness of the diagnostic method in ensuring continuous and reliable power delivery, even under adverse operating conditions, thereby enhancing the PV system's fault tolerance.

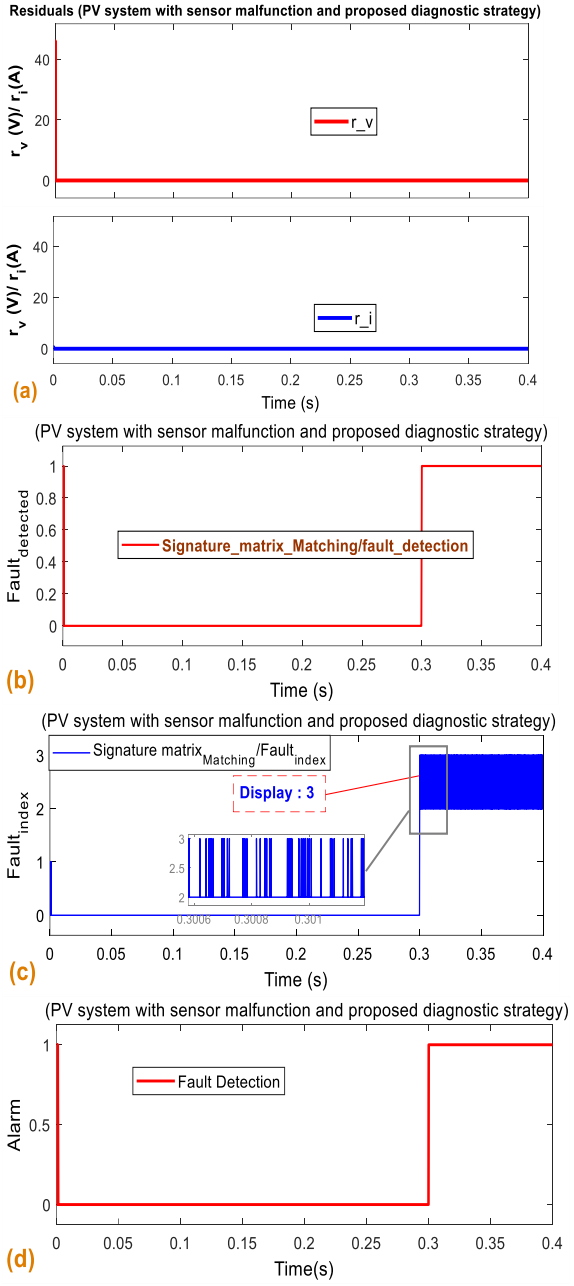

Fig. 20. illustrates the proposed diagnostic strategy, including: (a) the residual signals, (b) the fault detection indicator, (c) the identified fault index, and (d) the generated alarm signal

This figure 20 (a, b) illustrates the internal diagnostic mechanism based on residual generation and EKF estimation. The residuals, detection logic, fault index and alarm signal demonstrate how the system can detect faults rapidly and accurately, often within milliseconds. Not only does the EKF act as a state estimator, but it also acts as a fault detector, generating residuals that are highly sensitive to abnormal behaviour. Adaptive thresholds and signature-based classification enhance reliability, and real-time alarms enable immediate corrective action. This demonstrates that the EKF is not just a filtering tool, but an active monitoring agent that ensures safety and operational continuity.

Residuals r_v and r_i: Initially spike at startup (t ≈ 0s) then remain nearly zero throughout, reflecting high estimation accuracy by the EKF and minimal deviation between measured and estimated values:

Fault Detection Signal: Shows brief activation at t ≈ 0s, then a distinct and accurate detection at t ≈ 0.4s, confirming effective fault identification.

Fault Index (Signature Matching): The diagnostic module outputs a fault index signal, which indicates the type or location of fault. As shown in the figure, the index switches from 0 to 2 and then to 3 around t ≈ 0.3–0.4s. This confirms not only detection, but successful fault classification.

Alarm Triggered The alarm (signal turns to 1) is also triggered at approximately 0.3 seconds. This indicates that the system has not only detected the fault but has triggered an immediate alarm to take corrective action or notify the user.

The combined use of residuals, detection logic, signature-based fault indexing, and alarm signalling enables reliable, real-time detection and classification of sensor faults, supporting immediate response.

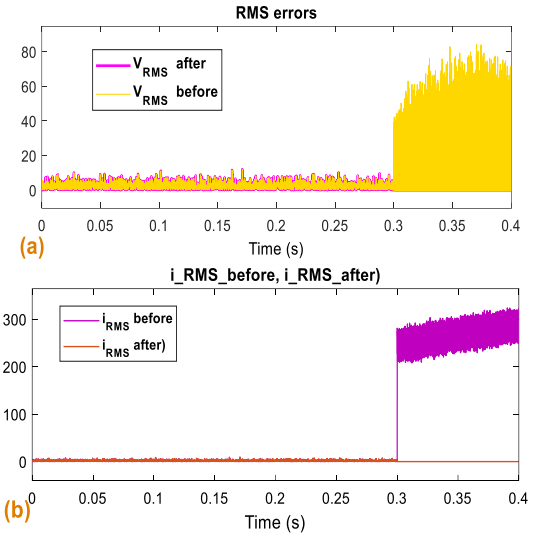

Fig. 21. RMS results before and after applying the diagnostic strategy

This figure 21 (a, b) quantitatively confirms the diagnostic effectiveness of the EKF strategy by comparing RMS voltage and current errors before and after fault detection.

Before diagnosis in Figure 21(a), the system suffers from large fluctuations due to faulty sensors. After applying EKF-based correction, the RMS errors drop by more than 99.9%, confirming outstanding estimation accuracy. This emphasizes EKF's value as a smart fault-tolerant observer, capable of restoring signal integrity and stabilizing the PV system under noisy, real-world conditions.

Effectiveness of the diagnostic strategy on system stability:

Figure 21 (a, b) show the RMS voltage and current values before and after the diagnostic strategy is applied, respectively. Figure 21(a) show that, prior to applying the diagnostic algorithm, the RMS voltage exhibits significant fluctuations and instability due to sensor malfunctions. After the diagnostic strategy is activated, the RMS voltage stabilises significantly, which confirms that the effects of faults on voltage measurements and control are mitigated.

Similarly, Figure 21(b) shows the RMS values for current. The current profile before the diagnostic intervention reveals significant variations and noise caused by the malfunctioning sensor. Afterwards, the RMS current exhibits a smooth, stable response, demonstrating the effectiveness of the proposed diagnostic and compensation method in restoring normal operation.

Figure 22 (a, b) a present the three-phase line-to-line voltages at Bus B1 under a sensor malfunction in the photovoltaic (PV) system. Despite the presence of the fault, the proposed diagnostic strategy successfully preserves the symmetry and amplitude of the voltage waveforms. The voltages maintain a consistent amplitude around ±20,000 V, confirming that the voltage regulation loop remains operational. This demonstrates the system's capability to ensure phase balance and voltage stability even when sensor data is unreliable. Figure 22 b demonstrates the EKF-driven diagnostic framework's ability to maintain three-phase voltage and current stability, even in the event of sensor faults. Despite disturbances at the sensor level, the system maintains waveform symmetry, phase balance and sinusoidal behaviour thanks to the EKF's real-time correction capabilities. By ensuring the MPPT algorithm receives valid data, the EKF guarantees effective control and maximised power delivery. Illustrates the three-phase current waveforms at Bus B1. A transient distortion is observed during the initial 0.05 seconds, indicating the disturbance introduced by the faulty sensor. However, the current waveforms quickly converge to balanced, sinusoidal patterns. This behaviour validates the effectiveness of the diagnostic and recovery mechanism in reestablishing normal operation and maintaining current symmetry.

Figure 22(c) shows the output voltage of the Voltage Source Converter (VSC) under the same fault scenario. Initially, the waveform exhibits large oscillations, but these gradually diminish as the control and diagnostic algorithms engage. The damping effect demonstrates the system's ability to dynamically stabilize the output, highlighting the contribution of the proposed strategy to fault resilience and voltage stability.

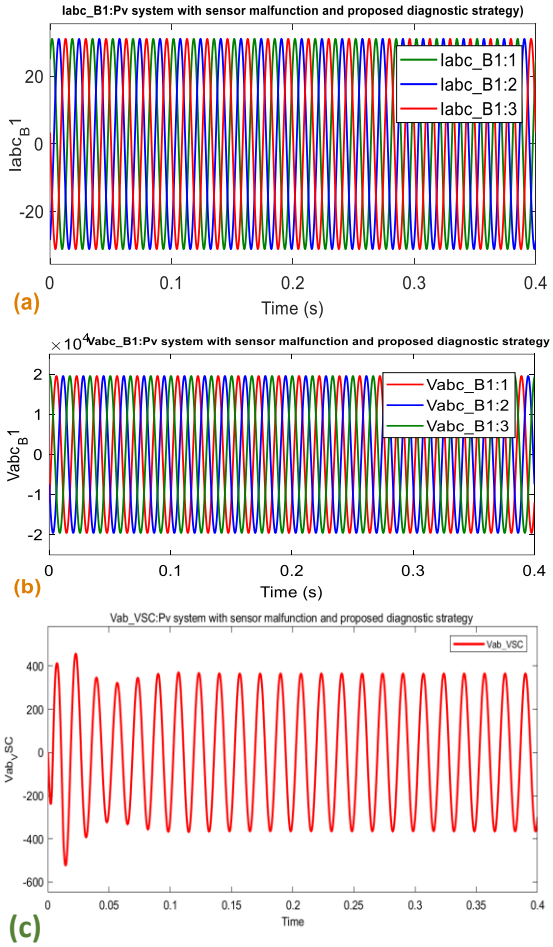

Fig. 22. (a)Three-phase voltages at the common bonding point in a PV system, (b) three-phase currents of a PV system at Bus B1, (c) VSC voltage in a PV system under sensor fault and application of corrective strategy

Table 3. Comprehensive quantitative comparison between diagnosed and undiagnosed PV system scenarios

Metric Performance	Before	After	Improvement
Voltage RMS Error (V)	~180	~0.11	▼ ~99.9%
Current RMS Error (A)	~250	~0.002	▼ ~99.9%
Detection Time (s)	—	~0.015	Real-time
Alarm Trigger	No	Yes (t ≈ 0.3s)	✓
Fault Classification	—	Yes (index 2,3)	Accurate
MPPT Efficiency (%)	< 65	> 95	Improved
Power Behaviour	Unstable	Stable	Enhanced quality
System Recovery (s)	None	< 0.02	Fast response

To assess the effectiveness of the proposed EKF-based fault diagnosis and switching strategy, the following table presents a detailed comparison of key performance indicators under two operating conditions: without any diagnostic mechanism and with the full diagnostic strategy implemented. The metrics include voltage and current estimation accuracy (RMS errors), response speed, power stability, and MPPT performance. The results demonstrate significant improvements in system robustness, power consistency, and fault handling capability when the diagnosis framework is activated. This comparison highlights the added value of the proposed diagnostic system across all performance axes, proving its relevance for real-time fault-tolerant control in photovoltaic applications. This comparison highlights the added value of the proposed diagnostic system across all performance axes, proving its relevance for real-time fault-tolerant control in photovoltaic applications.

Table 4. Impact of the proposed diagnostic strategy on system stability and power quality

Aspect	***Before Diagnostic Strategy***	***After Diagnostic Strategy***	***Improvement / Observation***
PV Power Fig. 3	Fluctuations, drops due to sensor fault	Stable tracking of irradiance	Improved power stability
Output Power Fig. 3	Slight degradation under fault	Maintained stable output	Reliable energy delivery
Voltage RMS (Fig. 4)	High fluctuations, instability	Stable voltage RMS	Enhanced voltage quality
Current RMS (Fig. 5)	Large oscillations, noise	Smooth and stable response	Improved current stability

This summarises the comparative performance of the PV system before and after the proposed diagnostic strategy was applied. As can be seen, the strategy significantly improves. the stability and quality of both the voltage and the current, while ensuring a reliable power output, even in the event of sensor faults.

7 CONCLUSION AND FUTURE RESEARCH DIRECTION

This study presents a nonlinear observer-based framework for fault diagnosis and fault-tolerant control of photovoltaic (PV) systems, built upon an Extended Kalman Filter (EKF). The contribution lies not in the EKF formulation per se, but in its systematic integration within a unified architecture that simultaneously performs state estimation, residual generation, adaptive fault detection, and real-time signal correction. This consolidation of functions addresses a key limitation in existing approaches, where estimation and diagnosis are typically treated as disjoint processes.

The proposed methodology has been assessed through extensive simulations under a range of sensor fault scenarios affecting PV voltage and current measurements. The results are unambiguous. Estimation errors are reduced by up to 99.9% in RMS terms; fault detection occurs within millisecond-scale time frames; MPPT efficiency remains consistently above 95%, even under degraded sensing conditions. Crucially, the signal reconfiguration mechanism triggered by residual evaluation ensures seamless substitution of corrupted measurements with EKF estimates, thereby maintaining control integrity without interruption.

Beyond numerical performance, the framework offers practical advantages. It improves power stability and operational reliability without introducing additional hardware redundancy or relying on data-intensive training procedures. This positions the approach as a viable solution for real-time PV monitoring, particularly in environments where computational efficiency and robustness are paramount.

Several directions emerge for further investigation. Extending the framework to accommodate multiple concurrent faults represents a natural progression, particularly in large-scale PV installations. The incorporation of parameter uncertainty and model mismatch into the estimation process would enhance robustness under real-world conditions. Experimental validation, beyond simulation, remains essential to confirm scalability and deployment feasibility. Finally, hybridization with advanced filtering strategies or data-driven techniques may offer additional gains in diagnostic sensitivity, especially in highly dynamic and uncertain operating regimes.

Source of funding: *This research received no external funding.*

Author contributions: *Research concept and design, H.H.C., A.I., K.L.; Collection and/or assembly of data, H.H.C., A.I., K.L.; Data analysis and interpretation, H.H.C., A.I., K.L.; Writing the article, H.H.C., A.I., K.L.; Critical revision of the article and final approval of the article, H.H.C., A.I., K.L.*

Declaration of competing interest: *The authors declares no conflict of interest.*

REFERENCES

1. Eason G, Noble B, Sneddon IN. On certain integrals of Lipschitz-Hankel type involving products of Bessel functions. Phil Trans R Soc Lond A 1955;247:529-551. https://doi.org/10.1098/rsta.1955.0005.
2. Hassan Q, Algburi S, Sameen AZ, Salman HM, Jaszczur M. A review of hybrid renewable energy systems: solar and wind-powered solutions: challenges, opportunities and policy implications. Results Eng. 2023;101621. https://doi.org/10.1016/j.rineng.2023.101621.

3. Jahangir MH, Cheraghi R. Economic and environmental assessment of solar-wind-biomass hybrid renewable energy system supplying rural settlement load. Sustain Energy Technol Assess. https://doi.org/10.1016/j.seta.2020.100895.
4. Gorjian S, Singh R, Shukla A, Mazhar AR. On-farm applications of solar PV systems. In: Photovoltaic solar energy conversion. Cambridge: Academic Press; 2020. https://doi.org/10.1016/B978-0-12-819610-6.00006-5.
5. Hijjawi U, Lakshminarayana S, Xu T, Fierro GPM, Rahman M. A review of automated solar photovoltaic defect detection systems: approaches, challenges and future orientations. Sol Energy 2023;266:112186. https://doi.org/10.1016/j.solener.2023.112186.
6. Joseph E, Vijaya Kumar PM, Mahinder Singh BS, Ching DLC. Performance monitoring algorithm for detection of encapsulation failures and cell corrosion in PV modules. Energies 2023;16(8):3391. https://doi.org/10.3390/en16083391.
7. Alrifai Y, Aguilera-Gonzalez A, Vechiu I. Estimation of diagnosis indicators for monitoring photovoltaic panels using artificial neural networks. 2024 International Conference on Control, Automation and Diagnosis (ICCAD), Paris, France, 2024. https://doi.org/10.1109/ICCAD60883.2024.10553687.
8. El-Banby GM, Moawad NM, Abouzalm BA, Abouzaid WF, Ramadan EA. Photovoltaic system fault detection techniques: A review. Neural Comput. Appl. 2023;35(35):24829-24842. https://doi.org/10.1007/s00521-023-09058-3.
9. Livera A, Theristis M, Micheli L, Fernandez EF, Stein JS, Georghiou GE. Operation and maintenance decision support system for photovoltaic systems. IEEE Access. 2022;10:42481-42496. https://doi.org/10.1109/ACCESS.2022.3168168.
10. Aboagye B, Gyamfi S, Ofosu EA, Djordjevic S. Investigation into impacts. Energy Sustain Dev. 2022;66:165-176. https://doi.org/10.1016/j.esd.2021.11.010.
11. Abdulla H, Sleptchenko A, Nayfeh A. Photovoltaic systems operation and maintenance. Renew Sustain Energy Rev. 2024;195:114342. https://doi.org/10.1016/j.rser.2023.114342.
12. Soomar AM, Hakeem A, Messaoudi M, Musznicki P, Iqbal A, Czapp S. Solar photovoltaic energy optimization and challenges. Frontiers in Energy Research. 202;10:879985. https://doi.org/10.3389/fenrg.2022.879985.
13. Yu C, Wang H, Yao J, Zhao J, Sun Q, Zhu H. A dynamic alarm threshold. Renew Energy. 2020;158: 13-22. https://doi.org/10.1016/j.renene.2020.05.127.
14. Ghazali SNAM, Sujod MZ. A comparative analysis of PV advanced fault detection. Electrica. 2023;23(1). https://doi.org/10.5152/electrica.2023.21035.
15. Spataru S, Sera D, Kerekes T, Teodorescu R. Diagnostic method. Sol Energy. 2015;119:29-44. https://doi.org/10.1016/j.solener.2015.06.004.
16. Abbas M, Chafouk H, Ardjoun SAEM. Fault diagnosis in wind turbine current sensors. Sensors. 2024;24(3):728. https://doi.org/10.3390/s24030728.
17. Yuan Z, Xiong G, Fu X. Artificial neural network for fault diagnosis of PV systems. Energies. 2022;15(22): 8693. https://doi.org/10.3390/en15228693.
18. Duer S, Valicek J, Paś J, Stawowy M, Bernatowicz D, Duer R, Walczak M. Neural networks in diagnostics. Energies. 2021;14(9):2719. https://doi.org/10.3390/en14092719.
19. Mansouri M, Trabelsi M, Nounou H, Nounou M. Deep learning-based fault diagnosis. IEEE Access 2021;9: 126286-126306. https://doi.org/10.1109/ACCESS.2021.3110403.
20. Alam Z, Khan MA, Khan ZA, Ahmad W, Khan I, Khan Q, Irfan M, Nowakowski G. Fault diagnosis strategy for a standalone photovoltaic system: A Residual formation approach. Electronics 2023;12: 282. https://doi.org/10.3390/electronics12020282.
21. Asadi S, Vafamand N, Moallem M, Dragičević T. Fault reconstruction. IEEE J Emerg Sel Top Power Electron. 2020;9(4):4606-4614. https://doi.org/10.1109/JESTPE.2020.3031340.
22. Criollo P, Ortiz L, Aguila A, Pavón W. A method based on SMC for PV systems. ETCM 2022. https://doi.org/10.1109/ETCM55056.2022.10016939.
23. Ahmad FF, Ghenai C, Hamid AK, Bettayeb M. Application of SMC for MPPT. Annu Rev Control. 2020;49:173-196. https://doi.org/10.1016/j.arcontrol.2020.04.012.
24. Zemali Z, Cherroun L, Hadroug N, Nadour M, Hafaifa A. Fault diagnosis-based observers using Kalman filters and Luenberger estimators: Application to the pitch system fault actuators. Diagnostyka. 2023; 24(1):1-13. https://doi.org/10.29354/diag/161307.
25. Kabalci E, Boyar A. Highly efficient interleaved solar converter controlled with extended Kalman filter MPPT. Energies. 2022;15(21):7838.7. https://doi.org/10.3390/en15217838
26. Pirashanthiyah L, Edirisinghe HN, De Silva WMP, Bolonne SRA, Logeeshan V, Wanigasekara, C. Design and analysis of a three-phase interleaved DC-DC boost converter with an energy storage system for a PV System. Energies. 2024;17:250. https://doi.org/10.3390/en17010250.
27. Mustafa A, Ramadan J, Gomaa MR, Al-Dhaifallah M, Rezk H. Environmental impacts. Sustainability 2020; 12(2):608. https://doi.org/10.3390/su12020608.
28. Aijaz M, Sakthivel K. ANFIS-based VSC. ICCSP. 2024;609-614. https://doi.org/10.1109/ICCSP55359.2024.10444272.
29. Ndeke CB, Adonis M, Almaktoof A. Basic circuit model of voltage source converters: Methodology and modelling. Appl Math. 2024;4(3):889-907. https://doi.org/10.3390/appliedmath4030048.
30. Simon D. Optimal state estimation: Kalman, H infinity, and nonlinear approaches. Hoboken: Wiley. 2006. https://doi.org/10.1002/0470045345.ch11.
31. Larik NA, Li MS, Wu QH. Enhanced fault detectionmedium-voltage DC distribution networks using extended Kalman filtering algorithm. IEEE Access. 2024;12:30329-30344. https://doi.org/10.1109/ACCESS.2024.3370479.
32. Zamzeer AS, Farhan MS, ALRikabi HT. Fault detection system of photovoltaic based on artificial neural network. Wasit Journal of Engineering Sciences. 202311(1)93-104. https://doi.org/10.31185/ejuow.Vol11.Iss1.399.
33. Raj V, Dotse SQ, Sathyajith M, Petra MI, Yassin H. Ensemble machine learning for predicting the power output from different solar photovoltaic systems. Energies. 2023 16(2);671. https://doi.org/10.3390/en16020671.

Dr. Hanene Chaourar is a Researcher at the Applied Automation and Industrial Diagnostics Laboratory, Faculty of Science and Technology, University of Djelfa, Algeria, where she has been conducting research since 2018. She obtained her Baccalaureate in Experimental Sciences in 2012, a B.Sc. in Industrial Computer Media Electronics in 2015 from Al-Bashir Al-Ibrahimi University, Algeria, and a M.Sc. in industrial computing in 2017 from the same university. Her bachelor's project focused on second-order band-pass and band-stop filters in sinusoidal regime with the development of a Matlab graphical interface to visualize frequency response using Bode diagrams. Her master's thesis was titled "Implementation of a Zero Correlation Zone (ZCZ) Code Generator on DSP for Asynchronous Applications in DS-CDMA Systems", proposing a new class of ternary ZCZ sequences with improved Bit Error Rate (BER) performance in DS-CDMA systems under AWGN and frequency non-selective fading channels. Her research interests include renewable energy systems, photovoltaic fault diagnosis, digital signal processing, and advanced control strategies. She has professional teaching experience at the University of Al-Ibrahimi University, Algeria.
e-mail: h.chaourare@univ-djelfa.dz

Dr. Abdelhamid Iratni (IEEE Senior Member) is a Professor of Electrical Engineering at the University of Mohamed El Bachir El Ibrahimi in Bordj Bou Arréridj, Algeria, where he has been teaching and conducting research since 2004. He currently serves as the Dean of the Faculty of Mathematics and Computer Science. He previously served as Chair of the Scientific Committee of the Electrical Engineering Department (2019–2025) and as Head of the Bachelor's and Master's Programs in Automatic Control (2015–2018). Dr. Iratni holds a B.Sc. (1999) and an M.Sc. (2003) from the University of Boumerdès, and a Ph.D. (2013) from Ferhat Abbas University of Sétif, Algeria. His research interests include nonlinear filtering, state estimation and control, biomedical and bioprocess engineering, industrial automation, and system reliability. He has published more than 50 peer-reviewed papers and has been a visiting researcher at the University of Strathclyde (UK), the University of Central Florida (USA), and the University of Coimbra / Institute for Systems and Robotics (Portugal). His academic leadership, research contributions, and international collaborations have established him as a recognized and influential figure in his field.
e-mail: iratni@univ-bba.dz

Dr. Laroussi Kouider received the Engineer degree in Electrical Engineering from the University of Djelfa, Algeria, in 1985, the Magister degree in Electrical Engineering from the National Polytechnic School of Algiers, Algeria, in 1998, and the Doctorate degree in Electrical Engineering from the National Polytechnic School of Algiers in 2007. He is currently a Professor with the Department of Electrical Engineering at Ziane Achour University of Djelfa. His research interests include power systems, renewable energy systems, fault diagnosis, intelligent control, optimization techniques, and electrical machine drives. He has authored and co-authored numerous scientific publications in these fields. e-mail: k.laroussi@univ-djelfa.dz